ADVANCED MATERIALS INTERFACES
www.advmatinterfaces.de

Plastic Antibodies Mimicking the ACE2 Receptor for Selective Binding of SARS-CoV-2 Spike

Alex D. Batista, Soumya Rajpal, Benedikt Keitel, Sandra Dietl, Beatriz Fresco-Cala,* Mehmet Dinc, Rüdiger Groß, Harald Sobek, Jan Münch, and Boris Mizaikoff*

Molecular imprinting has proven to be a versatile and simple strategy to obtain selective materials also termed "plastic antibodies" for a wide variety of species, i.e., from ions to macromolecules and viruses. However, to the best of the authors' knowledge, the development of epitope-imprinted polymers for selective binding of severe acute respiratory syndrome coronavirus 2 (SARS-CoV-2) is not reported to date. An epitope from the SARS-CoV-2 spike protein comprising 17 amino acids is used as a template during the imprinting process. The interactions between the epitope template and organosilane monomers used for the polymer synthesis are predicted via molecular docking simulations. The molecularly imprinted polymer presents a 1.8-fold higher selectivity against the target epitope compared to non-imprinted control polymers. Rebinding studies with pseudoviruses containing SARS-CoV-2 spike protein demonstrate the superior selectivity of the molecularly imprinted matrices, which mimic the interactions of angiotensin-converting enzyme 2 receptors from human cells. The obtained results highlight the potential of SARS-CoV-2 molecularly imprinted polymers for a variety of applications including chem/biosensing and antiviral delivery.

1. Introduction

Molecular imprinting strategies have been extensively applied for the synthesis of selective polymeric materials, especially for low-molecular-weight molecules.[1] The ability to selectively bind to a target species led to molecularly imprinted polymers (MIPs) also termed "plastic" or "artificial" antibodies.[2] They present remarkable advantages compared to natural antibodies such as resistance to variations on temperature, pH, and pressure, better mechanical performance, and simpler and cheaper synthesis.[3] Although MIPs are nowadays well established for small molecules, imprinting of macromolecules such as proteins is still particularly challenging due to their structural complexity, large molecular size, and conformational instability.[4–6] The polymer synthesis conditions (i.e., pH, solvents, temperature, stirring, etc.) affect protein conformation during the imprinting process, thereby resulting in low-affinity binding sites. The large number of functional groups of proteins also contributes to the formation of non-specific binding moieties, which limit MIP selectivity. Additionally, the need for high-purity proteins makes their use as templates costly. Considering the utility of MIPs for protein recognition acting as synthetic receptors, the need for novel approaches to overcome the present limitations is evident.

Epitope imprinting has emerged as a suitable alternative to improve protein recognition.[7–9] An epitope is a small fragment (i.e., up to twenty amino acids) of the protein structure that acts as an active binding site, which implies that the epitope is located at the surface of the protein and may potentially interact with the

A. D. Batista, S. Rajpal, B. Keitel, S. Dietl, B. Fresco-Cala, B. Mizaikoff
Institute of Analytical and Bioanalytical Chemistry
Ulm University
Albert-Einstein-Allee 11, 89081 Ulm, Germany
E-mail: alex.domingues-batista@uni-ulm.de; q72frcab@uco.es
A. D. Batista
Institute of Chemistry
Federal University of Uberlandia
Av. Joao Naves de Ávila 2121, Uberlândia 38400-902, Brazil

The ORCID identification number(s) for the author(s) of this article can be found under https://doi.org/10.1002/admi.202101925.

DOI: 10.1002/admi.202101925

S. Rajpal
Department of Biochemical Engineering and Biotechnology
Indian Institute of Technology Delhi
Hauz Khas, New Delhi 110 016, India
M. Dinc, B. Mizaikoff
Hahn-Schickard
Sedanstraße 14, 89077 Ulm, Germany
R. Groß, J. Münch
Institute of Molecular Virology
Ulm University Medical Center
Meyerhofstr. 1, 89081 Ulm, Germany
H. Sobek
Labor Dr. Merk & Kollegen GmbH
Beim Braunland 1, 88416 Ochsenhausen, Germany

corresponding receptors.[10] Epitope imprinting requires identifying those active protein sites, synthesizing the epitope peptide, and using it as a template for molecular imprinting.[9] The resulting MIP may then recognize the entire target protein via binding of the selected epitope region to the imprinted moieties at the surface of the MIP. This approach overcomes the drawbacks of using entire proteins as templates, as the epitope structure is simpler, more resistant to the synthesis conditions, and can be more easily removed from the resulting polymer matrix. Additionally, epitope peptides can be custom synthesized and are significantly cheaper versus native proteins. Furthermore, epitope imprinting is an attractive approach to produce imprinted materials for virus recognition.[11,12] Next to the advantages mentioned above, using epitopes as templates—as in the present study—also prevents direct contact with infectious viruses during MIP synthesis, and it does not require facilities with appropriate biological safety protocols.[13]

Coronaviruses are a group of RNA-enveloped viruses that can infect mammals and birds and may cause respiratory diseases that can range from mild to lethal problems. Severe acute respiratory syndrome coronavirus 2 (SARS-CoV-2) has been causing a severe outbreak worldwide since 2019 with millions of deaths and exceedingly high economic losses. SARS-CoV-2 is composed of four main structural proteins: nucleocapsid protein, envelope protein, membrane protein, and spike protein.[14] The latter is located on the virus surface and is the key interaction point to infect host cells. Hence, substantial attention has been attributed to the SARS-CoV-2 spike protein due to its role in receptor binding. Angiotensin-converting enzyme 2 (ACE2) is the human receptor for SARS-CoV-2, and promotes the entry of the virus into cells.[15,16] Therefore, the investigation of compounds that may interact with ACE2 and subsequently block SARS-CoV-2 infections is one of the most promising approaches to treat and prevent such virus infections.[17,18] Consequently, a variety of natural products have been identified that could act as therapeutic agents against SARS-CoV-2 via blocking of the spike protein sites. However, identifying such molecules is a complex task involving extensive computational simulations, extraction, isolation, and purification of the target compounds in sufficient quantities to perform affinity and antiviral experiments.[19–21] Hence, molecular imprints are a tool with substantial potential to obtain synthetic materials that may act similar to natural inhibitors by selectively interacting with specific sites of viruses, and consequently blocking the infection. Organic molecularly imprinted polymers for SARS-CoV-2 recognition were recently presented using the receptor-binding domain of SARS-CoV-2 and the nucleoproteins as templates on the molecular imprinting process. [22,23] In this context, nanomaterials have also been presented as promising alternative approaches to treat viral infections through different strategies as recently reviewed.[24,25]

Consequently, the present study aimed at designing and synthesizing the very first silane-based silica core/shell MIPs using an epitope peptide from the SARS-CoV-2 spike protein as a template, which could then act as a synthetic ACE2 receptor and bind to SARS-CoV-2.

2. Results and Discussions

2.1. Identification of the Epitope Template

The identification of the epitope employed as a template is extremely important to achieve selective polymers for the whole protein or virus. The epitope must be located at the protein surface and available to interact with external receptors. SARS-CoV-2 presents an envelope with homotrimeric spike glycoprotein composed of S1 and S2 subunits in each monomer that binds to cellular receptors. The initial SARS-CoV-2 infection step occurs through the interaction of the virus spike protein with angiotensin-converting enzyme 2 (ACE2) from human cells, which is the entry point for SARS-CoV-2. The structure of the receptor-binding domain (RBD) of the spike protein of SARS-CoV-2 when bound to the cell ACE2 receptor was previously elucidated, as presented in **Figure 1**,[15,16] which provides information to identify a suitable epitope candidate for molecular imprinting.

The epitope template was selected based on the maximum contacting residues with ACE2. A peptide comprising 17 residues (F486–G502) was selected, which presents ten contact moieties with ACE2 during interaction with the following amino acid sequence: FNCYFPLQSYGFQPTNG.[15]

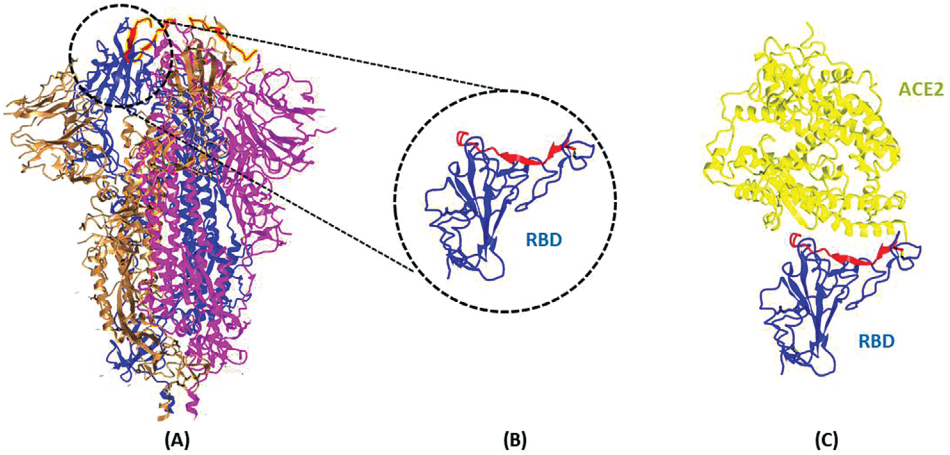

Figure 1. A) Overall structure of SARS-CoV-2 spike protein (Protein Data Base code 6VXX); B) receptor-binding domain with selected epitope highlighted in red; C) receptor-binding domain bound to ACE2 receptor (Protein Data Base code 6M0J).

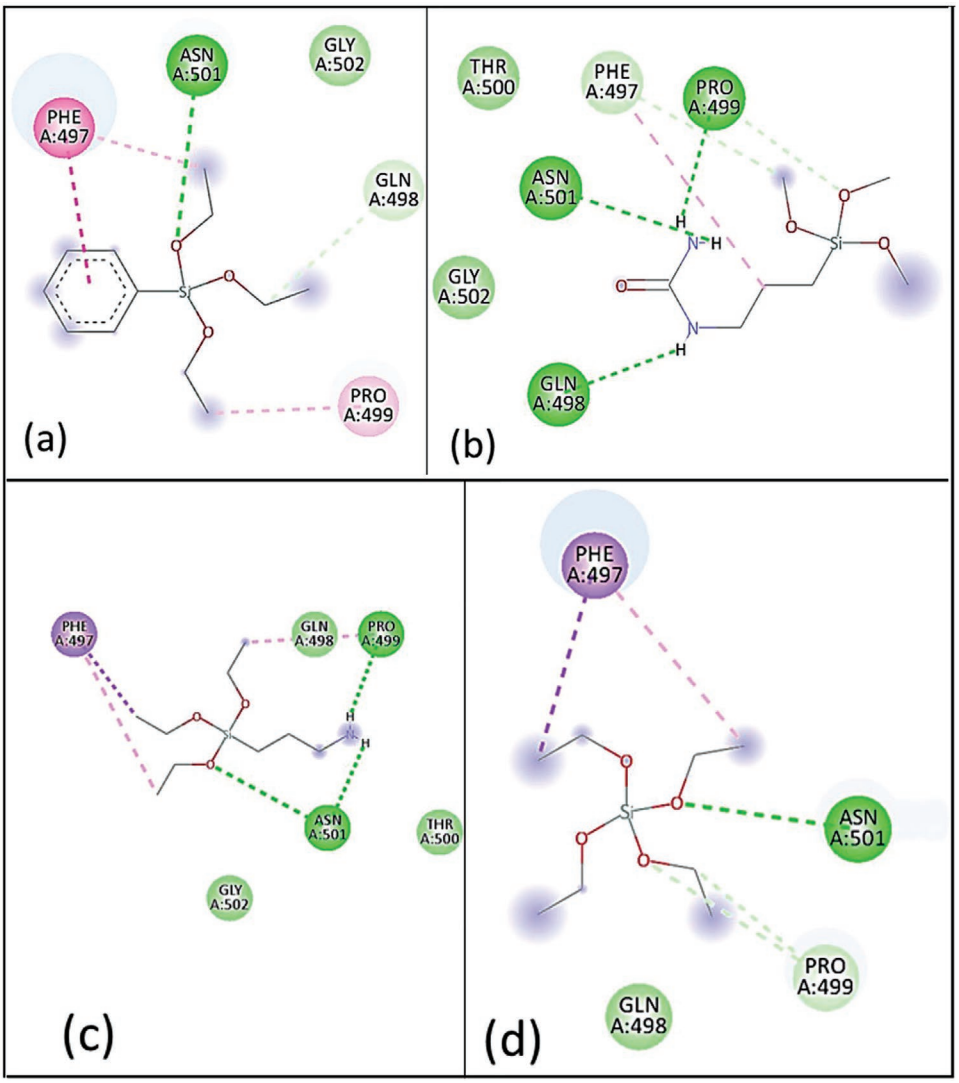

Figure 2. 2D interaction map representing the nature of interactions with the peptide at multiple residues. Green dotted lines represent hydrogen bonding, dark pink represents π–π bonds interactions, light pink lines show π–alkyl interactions, and purple lines indicate π–sigma interactions. Blue areas represent solvent-accessible surfaces. Green highlighted residues represent van der Waals interactions. a) PTES, b) UPTMS, c) APTES, and d) TEOS.

2.2. Computational Simulations

The SARS-CoV-2 epitope target is composed of 17 amino acids with different chemical functions. Six residues present hydrophobic side chains (three phenylalanine, two tyrosine, and one leucine), and five of which are aromatic, six residues present polar amino-functionalized side chains (two asparagine, two glutamine, one serine, and one threonine). Based on the epitope amino acid composition, phenyltriethoxysilane (PTES), 3-aminopropyltriethoxysilane (APTES), ureidopropyltrimethoxysilane (UPTES), and tetraethylorthosilicate (TEOS) were selected as functional monomers to cover a wide range of chemical interactions with the epitope template and were used on the theoretical simulations. We report for the first time, modeling of four organosilane monomers with a target SARS-CoV-2 epitope to substantiate the monomer–template complex formation in a pre-polymerization mixture. The qualitative assessment of each complex is based on the assigned quantitative score intended to correlate with the free energy of binding.[26] The basic framework and scoring function of Autodock is used for docking and revealing the dynamics of the monomer peptide interactions in the multicomponent system.

The principal analysis of the docking outcomes for MIP development is fundamentally different from that used for drug design. Unlike drug design approaches, which start with screening lead compounds with the strongest binding affinity to a targeted active site of a protein, molecular imprinting aims at effectively mimicking antigen–antibody interactions forming a complex resulting from multipoint noncovalent (i.e., weak) interactions. Therefore, we consider the free energy of binding of each monomer relative to the entire protein and all the binding modes in a fixed energy range. In this way, we analyze similar binding affinities of different monomers at multiple residues and map the interactions to cover the entire epitope.

The monomers used in this study yielded binding affinities in the range of −2.05 to −3.31 kcal mol^{-1}. The molecular and monomer-peptide interactions were modeled for each monomer based on the highest docking score (**Figures 2** and **3**).

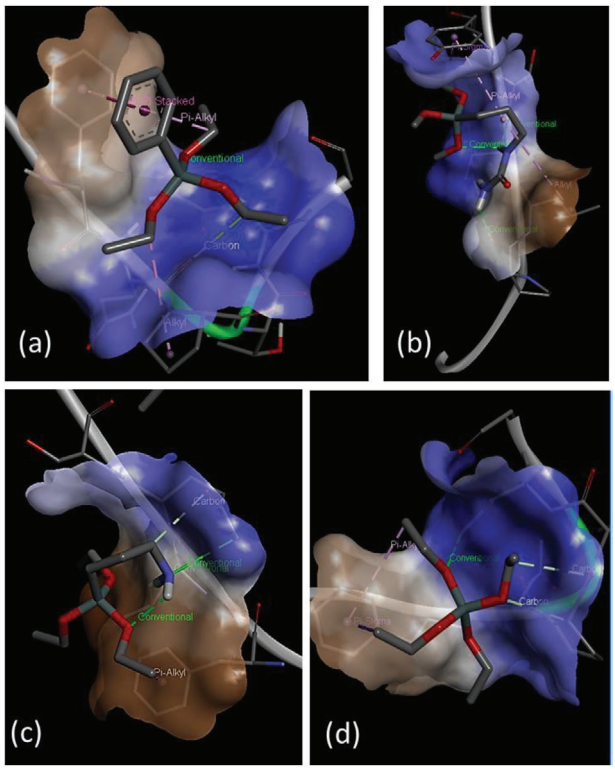

Figure 3. Representation (3D) of the nature of interactions of monomers: a) PTES, b) UPTMS, c) APTES, and d) TEOS with the peptide at multiple residues. Green dotted lines represent hydrogen bonding, dark pink represents π–π bonds interactions, light pink lines show π–alkyl interactions, and purple lines indicate π–sigma interactions. Blue and brown areas mark the hydrophilic and hydrophobic surfaces of the peptide, respectively.

Considering a large number of docking runs, first the mean binding energies of the first cluster rank as obtained in the clustering histogram were used to compare monomer–peptide affinities assigned by the empirical scoring function of Autodock (**Table 1**). As analyzed then during repeated docking studies, the PTES monomer has always yielded the lowest binding energy indicating the highest affinity with the peptide. The choice of this monomer is predominantly based on its interactions with the hydrophobic residues of the peptide (Figure 2a). The peptide contains three phenylalanine (PHE) and two proline (PRO) residues contributing to the major interactions with PTES, which are predominantly stacked π–π interactions and π–alkyl interactions, respectively. The polar hydroxyl groups interact with the asparagine (ASN) and glutamine (GLN) through hydrogen bonding. Interestingly, the molecular models show GLN and PRO residues forming carbon–hydrogen bonds and alkyl-based interactions with the ethoxy side chains of PTES, respectively (Figure 2a).

Table 1. Binding energy of selected monomers with SARS-CoV-2 epitope.

Monomer	Binding energy (single monomer docking) [kcal mol^{-1}]
Phenyltriethoxysilane (PTES)	−3.31
Ureidopropyltrimethoxysilane (UPTMS)	−2.64
3-Aminopropyltriethoxysilane (APTES)	−2.05
Tetraethylorthosilicate (TEOS)	−2.45

Considering that organosilanes readily undergo reactive hydrolysis during the formation of crosslinked polymer networks, it is obvious to expect the silanol groups (—Si—OH) to participate in non-covalent interactions in the pre-polymerization complex. However, the differential rate of hydrolysis for each type of monomer, which is also affected by the presence of the peptide in solution may facilitate interactions of the alkoxy groups in the monomers to coexist in solution. These can directly impact the preservation of peptide conformation during the imprinting process. The latter are unique interactions possible only in the case of MIPs and not NIPs, thus determining the resulting selectivity factor.

In the case of UPTMS, the urea moiety is the main center involved via H-bonding with the peptide (Figure 2b). Moreover, the propyl chain interacts via van der Waals forces with the aliphatic amino acids (leucine (LEU), glycine (GLY)), and π–alkyl interactions with the aromatic amino acids (PHE, tyrosine (TYR)). The highly polar silanol groups in the case of UPTMS can form large, interconnected networks of H-bonds with asparagine, glutamine, serine, and tyrosine. Methyl side groups however form fewer carbon–hydrogen bonds with PHE, TYR, and GLN. Most of the interactions with this monomer are distributed over the neutral and hydrophilic residues, unlike PTES.

The ethyl side chains in APTES (like PTES) participate in a range of hydrophobic interactions such as alkyl, π–alkyl, and π–sigma interactions with amino acids like PRO, LEU, TYR, and PHE (Figure 2c). The polar amino group and the central propyl chain participate in H-bonding and van der Waals interactions, similar to UPTMS. Owing to the structural similarities, APTES shares the set of interactions with PTES and UPTMS, thus enhancing the overall strength of binding to the peptide.

TEOS is a typical representative of the silane-based monomers and is limited by the number of functional groups, unlike others. The main interactions are possible via the silanol and ethoxy groups (Figure 2d). The results with TEOS were only used for studying the interactions with the peptide and not for comparison with other monomers, provided its main role as a cross-linker. For the other monomers, we have analyzed the binding energy range of 3.31 to −2.05 kcal mol^{-1} via 2D interaction maps generated in the Discovery Studio Visualizer. This is represented by a color-coded map of the sequence indicating the multipoint interactions realizable with the peptide in solution (Figure 3). The unique complementarity to each residue, as predicted from the molecular models enabled the rational selection of monomers for the design of MIPs against the SARS-CoV-2.

For the functional monomers, the computed binding energies correlate well with the experimental results. For example, PTES has the highest affinity with the peptide. When applied in an optimized combination, the binding capacities of the MIPs may substantially improve, as evident in combination 1 versus 6.

2.3. Epitope Immobilization onto Silica Particles

The immobilization of the template at the surface of the silica particles improves the imprinting efficiency by positioning

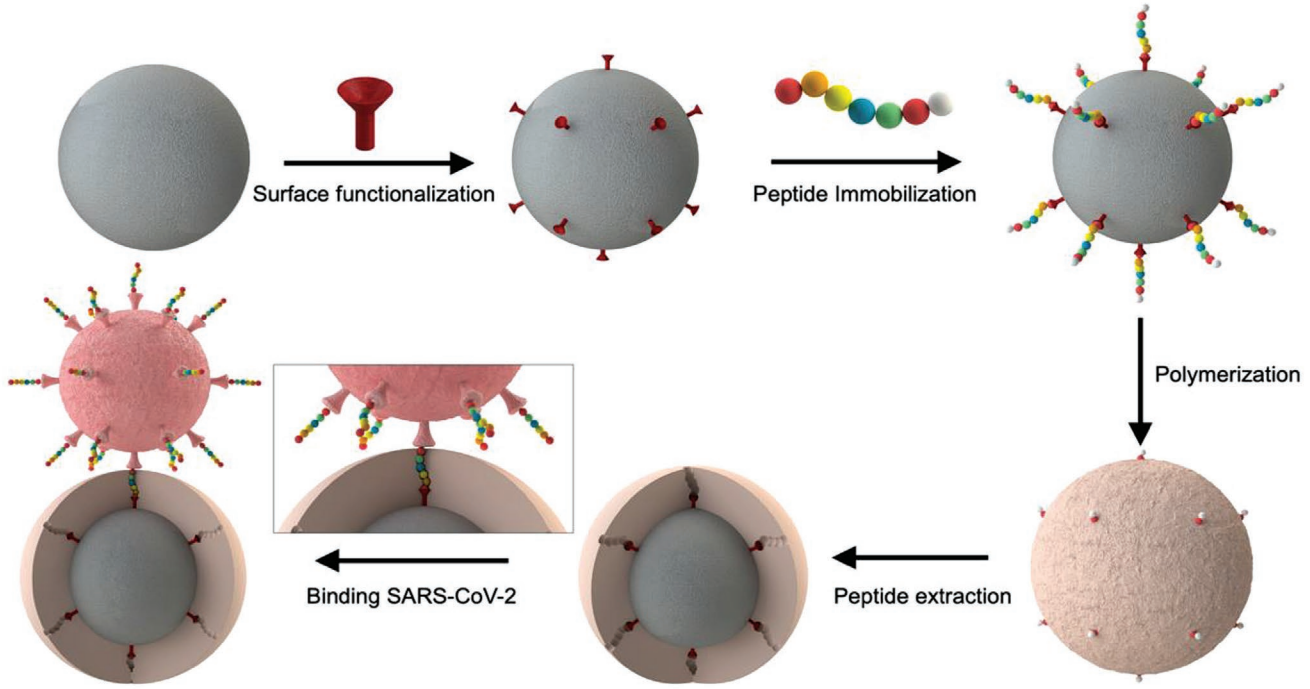

Figure 4. Synthesis scheme for peptide-imprinted core/shell particles for SARS-CoV-2.

the template around the silica particle prior to the polymerization. The SARS-CoV-2 epitope was immobilized at the surface of the silica particles functionalized with glutaraldehyde, which may react with several amino acids at the epitope, such as lysine, tyrosine, tryptophan, and phenylalanine.[27,28] Because the target SARS-CoV-2 epitope presents three phenylalanine and two tyrosine along the amino acid chain, the epitope can be anchored on the silica particle surface through five sites, which limits the free movement of the epitope during polymerization resulting in more effective imprinted moieties, as represented in the scheme in **Figure 4**. This approach was previously described for the immobilization of peptides serving as templates during MIP synthesis for the purification of human hemoglobin.[29]

The epitope concentration was monitored during the incubation with glutaraldehyde-functionalized silica particles to ensure its immobilization. After 1 h of incubation, 80% of the added epitope was immobilized at the silica particle surface.

2.4. MIP Design and Synthesis

The imprinted polymer particles were based on silica cores using organically modified silanes (aka ormosils), which present some advantages compared to purely organic-based polymers such as low reactivity in a variety of conditions (e.g., strong acids and bases, oxidizers, etc.), which results in a robust matrix that can be applied in a range of chemical and biochemical environments. Additionally, very well-defined binding moieties are achieved due to the rigid and highly crosslinked silane/silica structure, which results in superior selectivity compared to purely organic polymers that are more flexible. Silica also presents irrelevant swelling at different solvent conditions, which contributes to the maintenance of the size and shape of the binding moieties. Additionally, organosilica hybrid materials are readily obtained using molecular precursors that can take part in the hydrolysis and condensation reactions as the metal alkoxide, which is a versatile approach to adjust the selectivity of the MIP by selecting the most appropriate functional groups to interact with the epitope template.

Different monomer proportions were evaluated to achieve optimized imprinting efficiency (**Table 2**). The amount of TEOS on the polymer compositions was kept constant, as it acts as a cross-linker and presents only a minor influence on the intermolecular interactions between the epitope and the polymer due to the absence of functional groups. The PTES proportion was evaluated in a wider range due to the high number of amino acids with aromatic side chains on the SARS-CoV-2 epitope, which could improve imprinting efficiency through the π-interactions between polymer matrix and target epitope.

The MIP performance varied according to the polymer composition, as presented in **Figure 5**. While PTES presents the

Table 2. Molar ratio of monomers and cross-linker for MIP synthesis.

	APTES	PTES	UPTES	TEOS
Composition 1	20	10	10	60
Composition 2	10	10	20	
Composition 3	10	20	10	
Composition 4	7.5	25	7.5	
Composition 5	5	30	5	
Composition 6	0	40	0	

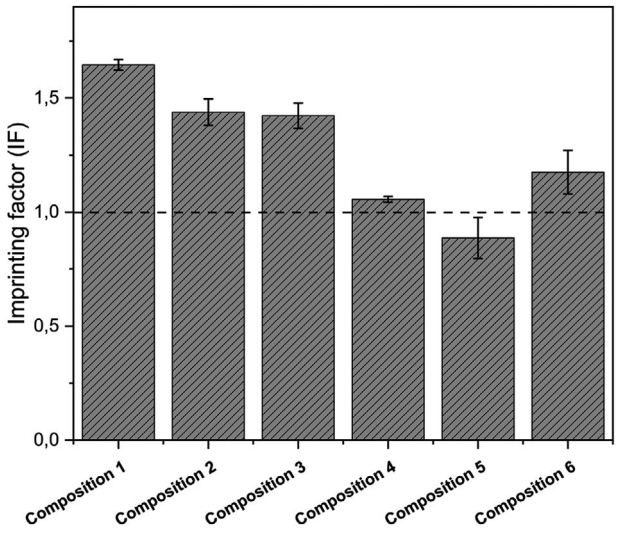

Figure 5. MIP performance using different functional silane molar ratios.

optimum binding energy (−3.13 kcal mol^{-1}) with the epitope template, a polymer composed only of PTES did not provide the best imprinting conditions, which indicates a synergic effect of the three selected monomers benefitting the resulting selectivity.

2.5. MIP/NIP Characterization

The polymers obtained at the optimum composition were physic and chemically characterized via scanning electron microscopy (SEM) and energy-dispersive X-ray spectroscopy (EDX). The surface chemical composition presented in **Table 3** confirms the modification of the silica particle surfaces through the synthesis steps. Glutaraldehyde-modified silica particles present higher content of C and O due to the glutaraldehyde functionalization of the surfaces of the particles and thus lower Si content. Silica particles covered by MIP and NIP presented higher C content due to the organic functional groups of the monomers employed for the polymer synthesis. The particles had a diameter of ≈0.5 µm, as shown in the SEM images in **Figure 6**. The MIP and NIP layer around the silica particle does not significantly change its diameter since it must be thin enough to avoid covering the immobilized epitopes on the silica particle surface, that are removed after the polymerization to create the imprinted sites.

Measurements of zeta potential of the particles at different steps of the synthesis of the polymers demonstrate the changes

Table 3. Surface composition (in atom %) of silica particles during MIP and NIP synthesis.

	C (at %)	O (at %)	Si (at %)
Bare silica particle	0.75	52.85	46.40
Glutaraldehyde-modified silica particle	1.30	54.91	43.79
NIP	2.28	49.94	45.25
MIP	2.20	49.09	46.34

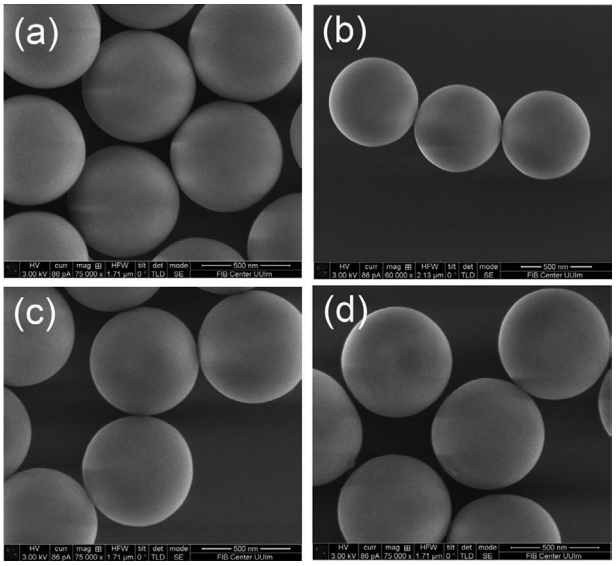

Figure 6. Scanning electron microscopy images of a) bare silica particles, b) after functionalization with glutaraldehyde, and after polymerization of the silane shell for c) MIP and d) NIP.

in the composition of the surface of the particles as presented in **Table 4**. Significant differences in the surface charges were observed after functionalization of the particles with glutaraldehyde. Despite MIP and NIP having the same chemical composition, MIP presented a lower zeta potential probably due to the different orientation of the functional groups on the surface during the formation of the imprinted sites.

2.6. Selectivity of the Polymers

The selectivity of the MIP and NIP was evaluated against three peptides with different amino acid compositions but similar lengths (peptide 1: MIVNDTGHETDENRA; peptide 2: TECSNLLLQYGSFCTQL; peptide 3: KLPDDFTGCV) and two human proteins (HAS: human serum albumin, HH: human hemoglobin). MIP and NIP presented a similar binding capacity for peptides and proteins indicating that the molecular imprinting for the SARS-CoV-2 epitope does not improve the adsorption of other peptides, as shown in **Figure 7**.

Besides the enhanced recognition ability against the epitope peptide used as the template, it is anticipated that the MIP also provides a higher affinity for the entire SARS-CoV-2 spike protein, and consequently, the SARS-CoV-2 virus. To investigate this, MIP and NIP particles were incubated with SARS-CoV-2-spike containing pseudoviruses and residual infectivity

Table 4. Zeta potential of silica particles during MIP and NIP synthesis.

	Zeta potential [mV]
Bare silica particle	−65.00 ± 0.31
Glutaraldehyde-modified silica particle	+3.53 ± 0.41
NIP	−0.95 ± 0.90
MIP	−13.2 ± 1.44

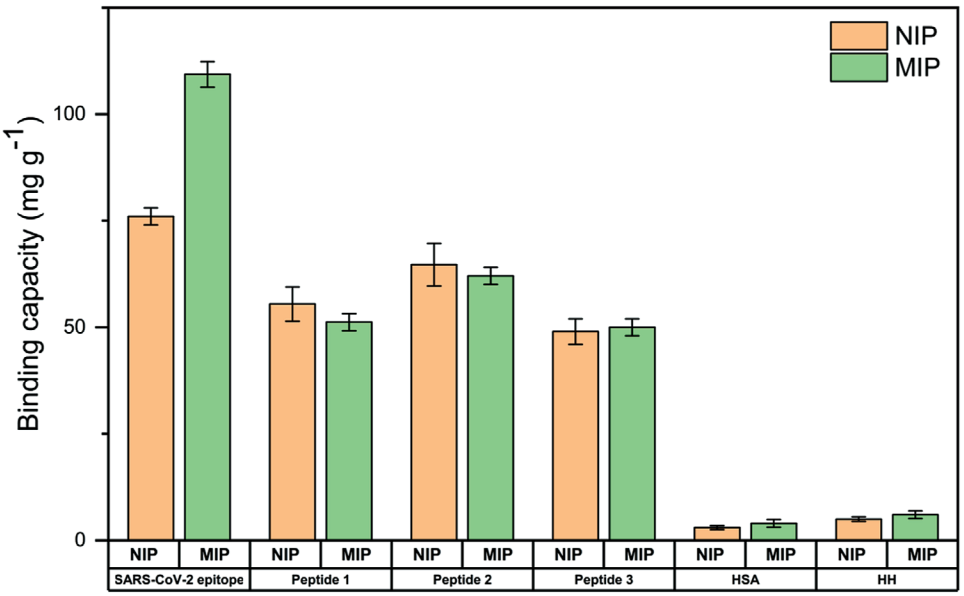

Figure 7. The binding capacity of MIP and NIP for the SARS-CoV-2 epitope and peptides of similar length.

in the supernatant quantified, revealing the ability of MIP/NIP to capture spike-containing viral particles. The MIP presented a significantly better affinity for the SARS-CoV-2 spike particles versus the NIP achieving an IF of 4.1, while an IF of 1.2 was observed for VSV-G glycoprotein particles, as shown in **Figure 8**. The same procedure was performed with phosphate-buffered saline (PBS) buffer as control (i.e., in absence of any polymers) and neutralizing agents for the spike protein (anti-S mAb, Bamlanivimab 35 μg mL^{-1}) and VSV-G (anti-G Hy, I1-Hybridoma supernatant) to confirm that infectivity is solely conferred by SARS-CoV-2-Spike or VSV-G in the respective pseudoviruses and may be blocked by specific agents entirely.

The performance of the developed MIP highlights their potential as "plastic antibody" for the treatment of SARS-CoV-2

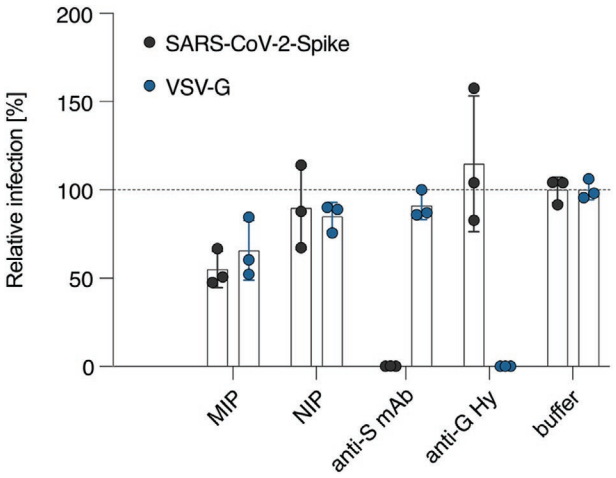

Figure 8. Relative infection of the supernatant after incubation with MIP, NIP, and neutralizing agents. Relative infection refers to luciferase activity in VeroE6 inoculated with pseudoviruses after the respective treatments, normalized to pseudoviruses treated with PBS only. Triplicate infections, error bars show SD.

via strategies including but not limited to drug-free therapeutics, whereby the MIPs may act as artificial ACE2 receptor targeting the active sites of SARS-CoV-2 spike protein thereby preventing the infection of cells. Furthermore, MIPs may be loaded with antiviral agents and act in a dual-mode approach combining drug delivery with binding to the spike protein. In the future, MIPs may also serve as an immunoprotective vaccine or a tool to improve chem/biosensors for the detection of SARS-CoV-2.

The obtained results also highlight the viability of using an epitope as a template for the molecular imprinting process to achieve excellent selectivity and recognition ability for an entire protein or virus. In addition, using peptides as templates has several advantages including easy and cheap access to customizable sequences versus native proteins, which are usually expensive and available only in small quantities, which limit their application as a template in molecular imprinting routines. Last but not least, using epitope peptides as templates does not require special facilities to handle pathogenic species during the MIP synthesis.

3. Conclusions

A silane/silica-based core/shell MIP that mimics ACE2 receptor and efficiently binds to SARS-CoV-2 spike RBD protein was developed. Computational simulations enabled the rational selection of the most suitable silane-based monomers via screening the interactions with the SARS-CoV-2 epitope, which resulted in MIPs of superior binding capacity for the selected peptide. The developed MIPs presented superior recognition abilities against pseudoviruses containing SARS-CoV-2 spike proteins, which highlights their substantial potential during the treatment and diagnosis of SARS-CoV-2 viruses. Since the developed MIPs mimic the ACE2 receptor and bind to the SARS-CoV-2 virus, they offer future perspectives on

drug-free therapeutics by blocking the infection of healthy cells. Finally, using an epitope peptide as the template during the molecular imprint synthesis renders this strategy safe, cheap, and easy to apply for a wide range of similar scenarios.

4. Experimental Section

Materials: PTES, APTES, UPTES, ammonium hydroxide solution (28.0–30.0% NH_3 basis), PBS buffer (pH 7.4), and glutardialdehyde were purchased from Sigma Aldrich (Steinheim, Germany). TEOS was obtained from Merck (Darmstadt, Germany). The custom peptides (FNCYFPLQSYGFQPTNG, MIVNDTGHETDENRA, and TECSNLLLQYGSFCTQL) were obtained from GenScript (Leiden, The Netherlands).

For the production of VSV pseudo particles expressing SARS-CoV-2 Spike (Wuhan Hu-1) or VSV-G (VSV serotype Indiana), HEK293T cells were transfected with expression plasmids as described previously.[30] One day after transfection, cells were inoculated with VSV*ΔG-FLuc and incubated for 1–2 h at 37 °C. VSV*ΔG-Fluc is a replication-deficient VSV vector in which the genetic information for VSV-G was replaced by genes encoding two reporter proteins, enhanced green fluorescent protein, and firefly luciferase (FLuc), and was kindly provided by Gert Zimmer, Institute of Virology and Immunology, Mittelhäusern, Switzerland.[31] The inoculum was removed, cells were washed with PBS and fresh medium containing anti-VSV-G antibody (I1-hybridoma cells; ATCC CRL-2700) to block residual VSV-G particles added when producing Spike-containing pseudo particles (not for VSV-G containing pseudo particles). After 16–18 h, the supernatant was collected and centrifuged (2000× *g*, 10 min, room temperature) to clear cellular debris. Samples were then aliquoted and stored at −80 °C.

Equipment: The morphology of the particles and their composition were investigated using a Quanta 3D FEG SEM equipped with a focused gallium ion beam (FIB) (FEI Corp., Eindhoven, The Netherlands), and an EDX detector (Apollo XV SDD, EDAX). Peptide detection was performed in a Specord S600 UV/Vis spectrophotometer (Analytik Jena). Zeta potential measurements were performed with a Zetasizer NANO ZSP (Malvern, Herrenberg, Germany).

Computational Simulations: The structural files for PTES, APTES, UPTMS, and TEOS were obtained from PubChem databank. The epitope/peptide structure (FNCYFPLQSYGFQPTNG) was extracted from the crystal structure of the SARS-CoV-2 receptor-binding domain (ID:7JMO) using UCSF Chimera.[32] Autodock tools were used for molecular docking. Autodock is probably the most commonly used open-source molecular docking software based on the AMBER force field suitable for proteins, nucleic acids, and other organic molecules.[33]

The ligand files were converted to pdbqt files after setting the torsional degrees of freedom based on the detected rotatable bonds. For docking of silane molecules, the parameters for Si were added in the AD4.1_bound and AD4_parameters data files (see the Supporting Information). Polar hydrogens were added to the peptide. Any water molecules were removed. A grid box of the dimensions 62 × 98 × 66 Å was centered around the peptide. The number of energy evaluations was set to the maximum (25 million evals) to improve the reproducibility and accuracy of the calculations. Furthermore, the number of docking runs was set to 100, specified by the ga_run parameter. For molecular docking, the Lamarckian Genetic Algorithm (LGA) was used. Docking results were analyzed using BIOVA Discovery Studio Visualizer software and UCSF Chimera.[32,34]

Silica Particle Synthesis and Functionalization: Silica particles were synthesized based on the Stöber method.[35] Briefly, ethanol (70 mL), ammonia (40 mL), and deionized water (20 mL) were added into a 250-mL round-bottom flask and stirred at 600 rpm by 5 min followed by the addition of TEOS (10 mL). The mixture was stirred for 20 h at 600 rpm and at room temperature (22 °C). The obtained silica particles suspension was centrifuged at 6500 rpm for 10 min and washed with one portion of ethanol (≈30 mL) and three portions of water (≈30 mL). The silica particles were dried in a vacuum oven at 40 °C and 200 mbar for 48 h.

Amino functionalization of the silica particles was performed as follows: silica particles (300 mg) were suspended in water (15 mL) in an ultrasonic bath for 30 min, followed by the addition of APTES (105 µL) and stirring at 600 rpm for 30 min. The amino-functionalized particles (NH_2-SP) were washed three times with deionized water to remove unreacted APTES.

Glutaraldehyde functionalization was performed by resuspending NH_2-SP in deionized water (15 mL) followed by the addition of glutaraldehyde (180 µL) and stirring at 600 rpm for 30 min. Glutardialdehyde-functionalized silica particles (Glut-SP) were washed with three portions of deionized water and dried in a vacuum oven at 40 °C and 400 mbar overnight.

Synthesis of MIP and NIP: The MIP synthesis consisted of three steps. I) immobilization of the epitope template on the surface of the Glu-SP: Glu-SP (30 mg) were resuspended in PBS buffer (5.0 mL, pH 7.4), and peptide solution (300 µL, 10 mg mL^{-1}) was added into the suspension and incubate by 1 h under 700 rpm stirring. II) Silica-based MIP synthesis: different molar ratios of TEOS, APTES, PTES, and UPTES were added into the Glu-SP suspension with immobilized epitopes and incubated for 80 °C for 80 min. III) Template removal: MIP particles were washed six times with HCl solution (30 mL, 0.1 mol L^{-1}). The NIP was synthesized at identical conditions without the addition of the epitope template.

Binding Studies: The binding studies were performed as follows: MIP or NIP (10 mg) were suspended into PBS buffer (2 mL, pH 7.4) and kept under stirring for 10 min, followed by the addition of the peptide solution (50 µL, 1 mg mL^{-1}). The mixture was kept under constant stirring in a rocking platform for 1 h at room temperature. The particles were separated by centrifuging at 5500 rpm for 10 min. The supernatant was analyzed in a Uv/Vis spectrophotometer.

For pseudovirus capture assay, VeroE6 were seeded in 96-well plates one day prior (6000 cells/well). Pseudovirus was then added to particles at twofold dilution and incubated for 1 h on a rocking platform at room temperature. Particles were then separated by centrifuging at 5500 rpm for 10 min. The supernatant was then added to VeroE6 at tenfold dilution. After an incubation period of 16–18 h, transduction efficiency was analyzed. For this, the supernatant was removed, and cells were lysed by incubation with Cell Culture Lysis Reagent (Promega) at room temperature. Lysates were then transferred into white 96-well plates and FLuc activity was measured using a commercially available substrate (Luciferase Assay System, Promega) and a plate luminometer (Orion II Microplate Luminometer, Berthold). For analysis of raw values (RLU/s), the background signal of an uninfected plate was subtracted, and values normalized to pseudovirus incubated in PBS only (without MIP/NIP).

Acknowledgements

This work was in part supported by the Ministerium für Wissenschaft, Forschung und Kunst (MWK) Baden-Württemberg, Germany, under the Program "Special Measures against the SARS-CoV-2 Pandemic." A.D.B. and B.F.-C. are also thankful to the Alexander Von Humboldt Foundation for their postdoctoral fellowship enabling the research stay at the Institute of Analytical and Bioanalytical Chemistry, Ulm University, Germany. R.G. is part of the International Graduate School in Molecular Medicine (IGradU) of Ulm University. S.R. thanks the German exchange service (DAAD) for the fellowship award that supports research work at Ulm University.

Open access funding enabled and organized by Projekt DEAL.

Conflict of Interest

The authors declare no conflict of interest.

Data Availability Statement

Research data are not shared.

Keywords

core–shell molecularly imprinted polymers, coronavirus, epitope imprinting, molecularly imprinted polymers simulations, molecularly imprinted polymers, peptide imprinting, synthetic receptors

Received: October 6, 2021
Revised: November 16, 2021
Published online: January 5, 2022

[1] L. Chen, X. Wang, W. Lu, X. Wu, J. Li, *Chem. Soc. Rev.* **2016**, *45*, 2137.
[2] J. Wackerlig, P. A. Lieberzeit, *Sens. Actuators, B* **2015**, *207*, 144.
[3] A. Poma, A. P. F. Turner, S. A. Piletsky, *Trends Biotechnol.* **2010**, *28*, 629.
[4] M. Dinc, C. Esen, B. Mizaikoff, *TrAC, Trends Anal. Chem.* **2019**, *114*, 202.
[5] J. Kalecki, Z. Iskierko, M. Cieplak, P. S. Sharma, *ACS Sens.* **2020**, *5*, 3710.
[6] R. Xing, Y. Ma, Y. Wang, Y. Wen, Z. Liu, *Chem. Sci.* **2019**, *10*, 1831.
[7] H. Peng, Y. T. Qin, X. W. He, W. Y. Li, Y. K. Zhang, *ACS Appl. Mater. Interfaces* **2020**, *12*, 13360.
[8] A. Kushwaha, J. Srivastava, A. K. Singh, R. Anand, R. Raghuwanshi, T. Rai, M. Singh, *Biosens. Bioelectron.* **2019**, *145*, 111698.
[9] T. Khumsap, A. Corpuz, L. T. Nguyen, *RSC Adv.* **2021**, *11*, 11403.
[10] J. Huang, W. Honda, *BMC Immunol.* **2006**, *7*, 7.
[11] D.-F. Tai, C.-Y. Lin, T.-Z. Wu, L.-K. Chen, *Anal. Chem.* **2005**, *77*, 5140.
[12] C.-Y. Chou, C.-Y. Lin, C.-H. Wu, D.-F. Tai, *Sensors* **2020**, *20*, 3592.
[13] G. J. Soufi, S. Iravani, R. S. Varma, *Analyst* **2021**, *146*, 3087.
[14] A. Wu, Y. Peng, B. Huang, X. Ding, X. Wang, P. Niu, J. Meng, Z. Zhu, Z. Zhang, J. Wang, J. Sheng, L. Quan, Z. Xia, W. Tan, G. Cheng, T. Jiang, *Cell Host Microbe* **2020**, *27*, 325.
[15] J. Lan, J. Ge, J. Yu, S. Shan, H. Zhou, S. Fan, Q. Zhang, X. Shi, Q. Wang, L. Zhang, X. Wang, *Nature* **2020**, *581*, 215.
[16] Q. Wang, Y. Zhang, L. Wu, S. Niu, C. Song, Z. Zhang, G. Lu, C. Qiao, Y. Hu, K.-Y. Yuen, Q. Wang, H. Zhou, J. Yan, J. Qi, *Cell* **2020**, *181*, 894.
[17] C. J. Day, B. Bailly, P. Guillon, L. Dirr, F. E. C. Jen, B. L. Spillings, J. Mak, M. von Itzstein, T. Haselhorst, M. P. Jennings, *MBio* **2021**, *12*.
[18] C. G. Benítez-Cardoza, J. L. Vique-Sánchez, *Life Sci.* **2020**, *256*, 117970.
[19] K. Gopinath, E. M. Jokinen, S. T. Kurkinen, O. T. Pentikäinen, *Front. Chem.* **2020**, *8*, 1084.
[20] C. H. Kim, *Frontiers* **2021**, *12*, 1015.
[21] R. Chakravarti, R. Singh, A. Ghosh, D. Dey, P. Sharma, R. Velayutham, S. Roy, D. Ghosh, *R. Soc. Chem.* **2021**, *11*, 16711.
[22] A. Raziq, A. Kidakova, R. Boroznjak, J. Reut, A. Öpik, V. Syritski, *Biosens. Bioelectron.* **2021**, *178*, 113029.
[23] O. I. Parisi, M. Dattilo, F. Patitucci, R. Malivindi, S. Delbue, P. Ferrante, S. Parapini, R. Galeazzi, M. Cavarelli, F. Cilurzo, S. Franzè, I. Perrotta, V. Pezzi, F. Selmin, M. Ruffo, F. Puoci, *Nanoscale* **2021**, *13*, 16885.
[24] A. F. Nahhas, A. F. Nahhas, T. J. Webster, *Nanomedicine* **2021**, *16*, 1237.
[25] A. F. Nahhas, T. J. Webster, *J. Nanobiotechnol.* **2021**, *19*, 305.
[26] J. Li, A. Fu, L. A. Zhang, *Interdiscip. Sci. Comput. Life Sci.* **2019**, *11*, 320.
[27] A. F. S. A. Habeeb, R. Hiramoto, *Arch. Biochem. Biophys.* **1968**, *126*, 16.
[28] D. Hopwood, C. R. Allen, M. McCabe, *Histochem. J.* **1970**, *2*, 137.
[29] H. Bagán, T. Zhou, N. L. Eriksson, L. Bülow, L. Ye, *RSC Adv.* **2017**, *7*, 41705.
[30] M. Hoffmann, P. Arora, R. Groß, A. Seidel, B. F. Hörnich, A. S. Hahn, N. Krüger, L. Graichen, H. Hofmann-Winkler, A. Kempf, M. S. Winkler, S. Schulz, H.-M. Jäck, B. Jahrsdörfer, H. Schrezenmeier, M. Müller, A. Kleger, J. Münch, S. Pöhlmann, *Cell* **2021**, *184*, 2384.
[31] M. B. Rentsch, G. Zimmer, *PLoS One* **2011**, *6*, e25858.
[32] E. F. Pettersen, T. D. Goddard, C. C. Huang, G. S. Couch, D. M. Greenblatt, E. C. Meng, T. E. Ferrin, *J. Comput. Chem.* **2004**, *25*, 1605.
[33] G. M. Morris, H. Ruth, W. Lindstrom, M. F. Sanner, R. K. Belew, D. S. Goodsell, A. J. Olson, *J. Comput. Chem.* **2009**, *30*, 2785.
[34] D. Systèmes, *BIOVIA Discovery Studio Visualizer — Dassault Systèmes*, https://discover.3ds.com/discovery-studio-visualizer-download (accessed: May 2021).
[35] W. Stöber, A. Fink, E. Bohn, *J. Colloid Interface Sci.* **1968**, *26*, 62.